# Shoreline and Land Use Land Cover Changes along the 2004 tsunami-affected South Andaman Coast: Understanding Changing Hazard Susceptibility

Vikas Ghadamode[1,2], Aruna Kumari Kondarathi [1], Anand K Pandey[1,2] Kirti Srivastava[1]

1. CSIR- National Geophysical Research Institute, Hyderabad, 500007 India.

2. Academy of Scientific and Innovative Research (AcSIR), Ghaziabad 201002, India.

§ Corresponding author: Email address: akpandey@ngri.res.in

*Tel: +91-40-27012416*

**Abstract**

The 2004 tsunami affected the South Andaman coast, experiencing dynamic changes in the coastal geomorphology, making the region vulnerable. We focus on pre-and post-tsunami shoreline and Land Use Land Cover changes for 2004, 2005, and 2022 to analyse the dynamic change in hazard. We used GEBCO bathymetry data to calculate Run-up (m), arrival times (Min), and inundation (m) at a few locations using three tsunamigenic earthquake source parameters, namely the 2004-Sumatra, 1941-North Andaman, and 1881-Car Nicobar earthquakes. The Digital Shoreline Analysis System is used for the shoreline change estimates. The Landsat data is used to calculate shoreline and Land Use Land Cover (LULC) change in five classes, namely Built-Up Areas, Forests, Inundation areas, Croplands, and water bodies during the above period. We examine the correlation between the LULC changes and the dynamic change in shoreline due to population flux, infrastructural growth, and Gross State Domestic Product growth. India industry estimates the Andaman & Nicobar Islands losses exceed INR 10 billion during 2004, which would see a five-fold increase in economic loss due to a doubling of built-up area, a three-fold increase in tourist inflow, and a population density growth. The unsustainable decline in the forest cover, mangroves, and cropland would affect sustainability during a disaster despite coastal safety measures.

**Keywords: Geomorphology, Land use Land cover, Shoreline, Tsunami, Remote sensing**

## 1. Introduction:

The Coastal shorelines are dynamic and highly vulnerable to erosion and accretion caused by hydrodynamic, tectonic, geomorphic, and climate forcing, including tsunamis, cyclones, flooding, storm surges, wave action, wind and tide changes, and sea level variations (Nayak 2002; Boak &Turner 2005; Kumar et al., 2010; Mukhopadhyay et al., 2011). In addition to natural coastal processes, coastal resources are constantly under stress due to anthropogenic activities, such as industrialization, port construction, beach sand mining, garbage dumping, urbanization, trade, tourism, and recreational activities, which significantly impact the shoreline and results into damage to natural ecosystems (Yi et al., 2018; Davis, 2019). It is important to regularly monitor spatiotemporal along shorelines, Land use / Land Cover (LULC), and geomorphic features (Moran, 2003; Cooper et al., 2004; Scheffers et al., 2005; Jayakumar & Malarvannan, 2016). Several studies have analyzed various coastal processes, including mapping shoreline change, LULC change detection, and analysis of geomorphological landforms using satellite data. The temporal multispectral satellite data allow for the identification of regions undergoing erosion or accretion change (Misra and Balaji, 2015; Kumari et al., 2012; Tonisso et al., 2012; Murali et al., 2013; Sudha Rani et al., 2015; Rowland et al., 2022; Thiéblemont et al., 2021). The M 9.3 undersea earthquake on December 26, 2004, near the coast of Sumatra, Indonesia, triggered the Indian Ocean tsunami and caused massive destruction of the coastal ecosystem in the Andaman region (Sheth et al., 2006; Ramalanjaona, 2011). The shoreline and geomorphological changes of the 2004 Sumatra tsunami were analyzed using statistical techniques on remote sensing data (Kumari et al., 2012; Yuvaraj et al., 2014; Yunus and Narayana, 2015; Yunus et al., 2016).

Since the 2004 tsunami, the Andaman and Nicobar Islands have experienced notable population growth, infrastructural development, and flourishing tourism activities over the past decade (Yuvaraj et al., 2014). The development is profound in the south Andaman region. This

is a cause of concern for the tsunami vulnerability as the region is prone to large earthquakes and is a seismo-tectonically active plate boundary. In this study, we Compute Tsunami arrival times, run-up heights, and inundation extent along the south Andaman region. We also analyzed dynamic vulnerability using temporal and spatial changes in shoreline and LULC for the tsunami-affected areas (Velmurugan et al., 2006; Ghadamode et al., 2022). The analysis covers three time periods: 2004 (pre-tsunami), 2005 (post-tsunami), and 2022 (current state) of shoreline changes using multi-temporal Landsat data employing the End Point Rate (EPR) and Net Shoreline Movement (NSM) methods (Himmelstoss et al., 2021) and LULC changes. A relationship between LULC changes and vital socioeconomic factors such as population dynamics, tourism trends, and the Gross State Domestic Product (GSDP) is established to assess the potential future impacts of tsunamis in the region. The results would provide actionable insights to the policymakers, coastal planners, and stakeholders in disaster management and sustainable coastal development.

## 2. Study Area

South Andaman region, with ~1,262 km² area and a 413 km coastline, is the southernmost island of the Great Andaman, where most of the Andaman Island's population and infrastructure are centered. As per the 2011 Indian census, South Andaman has a population of 238,142 people, which increased to 266,900 in 2021 (estimate based on www.census2011.co.in). The most habitable areas in the eastern part of South Andaman are located on low lands at bay heads in addition to the higher slopes bordering bays and coastal flat lands (Ghosh et al., 2004), which experienced devastation and losses during the 2004 Tsunami (Fig. 1). We selected 13 locations, namely South Point in Port Blair, Rutland Island, Corbyn's Cove Beach, Madhuban Bay, Brichgunj, Chidiyatopu, Thirupatti Temple, Wandoorjetty, Bamboo Flat, Potatang, Shoal Bay, Radha Nagar, and Govinda Nagar (Fig. 1) for vulnerability assessment in the present study.

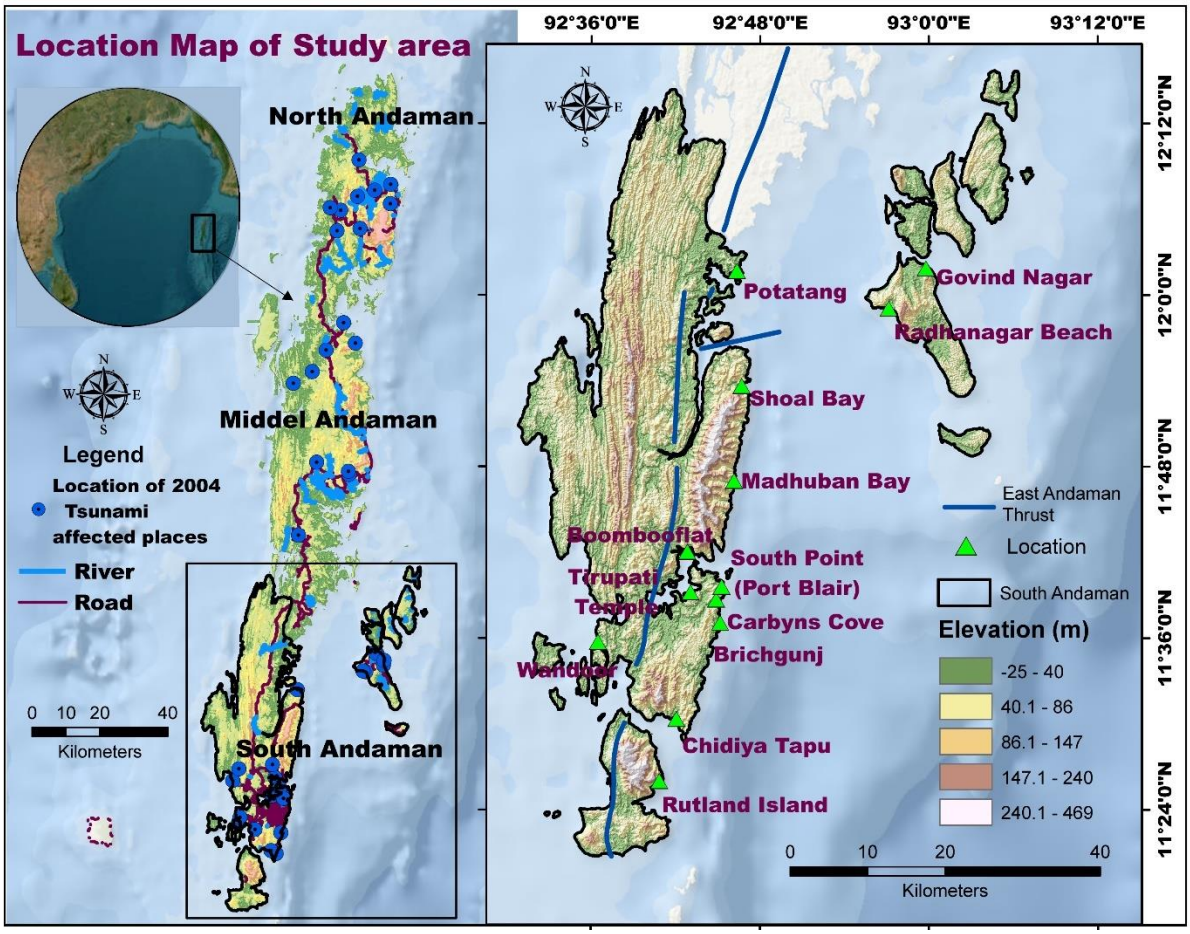


*Figure 1 Location Map of the South Andaman Region (*© Google Maps & © Google Earth*).*

The tectonic activity and weathering processes have influenced the region's topography growth and evolution (Curray, 2005; Bandopadhyay and Carter, 2017). The East Andaman Thrust, also called East Boundary Thrust, is a linear/curvilinear ~500 km long fault zone and is the locus of ongoing convergent and crustal deformation along the Sunda-Andaman plate boundary. This structure is pivotal in creating accretionary prisms within the outer-arc ridge of the Andaman and Nicobar subduction zones (Fig. 1; Bhat et al., 2023).

The structure-bound major geomorphological features in South Andaman include hills, valleys, beaches, mangroves, and coral reefs (Fig. 2a). The highest peak on the island is Mount Harriet, with approximately 1,200 m (3,937 feet) (southandaman.nic.in). The north-western and north-eastern parts of South Andaman are highly and moderately dissected, whereas the Southern part has low dissected structural hills and valleys (Fig. 2a, b, c, and d). The upper

slopes of the region are covered with high dissected structural hills with dense pristine forest (Fig. 2a). The slope ranges between 0 to 44.9 degrees, with lower slopes in the coastal region mostly inhibited and undergoing rapid coastline modification and Land Use Change. The North, Northeast, and Southern portions of South Andaman have the steepest slope and relief area, while the Eastern, Southeastern, and western parts have relatively lower slopes (Fig. 2b and c). The island has a rough coastline with various bays, inlets, and headlands (Fig. 2). The Younger coastal plain is a relatively flat and low-lying area adjacent to the coastline, which is formed through the accumulation of sediments brought by the ocean (Fig. 2e). A wave-cut platform, formed by the erosive action of waves, are flat or gently sloping rock surface are found along South Point coastlines in Port Blair (Fig. 2f). These platforms can be exposed at low tide, which gradually wear away the rock over time, are unique feature of rocky coastlines. Coral reefs along the coast contribute to forming sandy beaches and barrier islands (Reguero et al., 2018). Mangrove forests are found on coasts in South Andaman Island, primarily in the brackish water and muddy sediments lagoons and tidal zone (Fig. 2g). Mangroves are crucial in stabilizing coastal ecosystems and providing habitat for various species. Wandoor, Chidya tapu, and Sippighat are some notable locations of mangrove forests in South Andaman coastal areas. The coastal plains in south Andaman are dynamic and prone to tsunamis due to their location and active plate boundary. Therefore, studying shoreline change and LULC change is especially important because of the potential impacts on local communities and ecosystems.

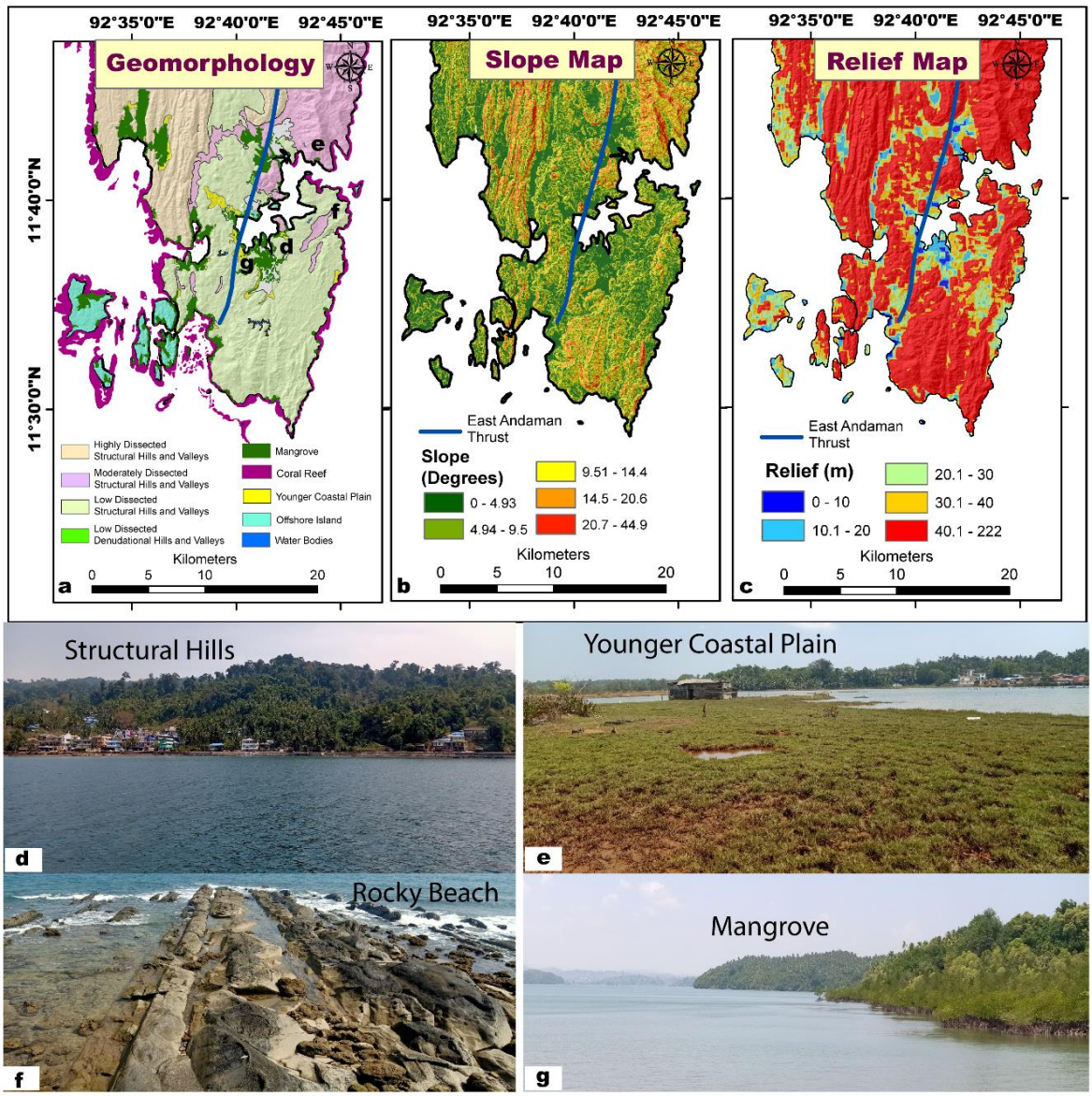


***Figure 2 (a)*** *Geomorphology,* ***(b)*** *Slope map,* ***(c)*** *Relief Map,* ***(d)*** *Structural Hills,* ***(e)*** *the younger coastal plain,* ***(f)*** *Rocky Beach with a wave-cut platform near south point, Port Blair,* ***(g)*** *Mangrove.*

## 3. Materials and Methods

It is imperative to generate a spatial dataset that may have a bearing on the dynamic changes to assess the vulnerability.

### 3.1 Data Used

Landsat satellite data, such as Thematic Mapper (TM) and Operational Land Imagery (OLI) sensor for the years 2004, 2005, and 2022, is used to analyze shoreline and monitor the LULC changes along the South Andaman coast in the present study. The Shuttle Radar

Topography Mission (SRTM) Digital Elevation Model (DEM) is used to prepare the study area's slope and relief map. We used the General Bathymetry Chart of the Ocean (GEBCO) for run-up and inundation studies along the south Andaman coastal areas (Table 1).

**Table 1:** Data used in the present study region

| Data | Purpose | Date & Year | Resolution | Sources |
|---|---|---|---|---|
| GEBCO bathymetry | Inundation and Run-Up | 2022 | 90 m | GEBCO (https://www.gebco.net/) |
| Landsat 5 TM, Landsat 8 OLI | LULC and Shoreline Change Analysis | 26-02-2004<br>27-01-2005<br>27-02-2022 | 30 m | USGS Earth Explorer |
| SRTM DEM | Slope, Relief | - | 30m | USGS Earth Explorer |
| Geomorphology | Geomorphology | - | 1:250k | bhukosh.gsi.gov.in |
| Socioeconomic data | Population,<br>Tourism,<br>Gross State Domestic Product (GSDP) | 1991-2021<br><br>2001-2020 | - | (censusindia.gov.in)<br>(Directorate of economics and statistics)<br>(Rbi.org.in) |

### 3.2 Tsunami Run-ups and Inundation

Several attempts have been made to model tsunamis to calculate inundation and determine run-up heights to evaluate their impact and hazards along mainland Indian coastal areas (Rani et al., 2011; Srivastava et al., 2021). However, despite experiencing historical tsunamis during the 31 December, 1881-Car Nicobar, 26 June, 1941-North Andaman, and the 26 December, 2004-Sumatra earthquakes, the south Andaman region is yet to be explored for scenario hazard assessment. We used the Tohoku University's Numerical Analysis Model for Investigation of Near field tsunamis (TUNAMI-N2) to simulate the tsunami run-ups and impact using finite-difference methods to solve shallow water wave equations, incorporating bathymetry, earthquake source parameters, and fault geometry (Imamura and Imteaz, 1995; Imamura, 1996). In deep-sea regions with longer wavelengths a coarse grid spacing to model linear effects is sufficient to resolve the wave with minimal error. As the tsunami wave propagates from deep to shallow waters, where the wavelength shortens and the amplitude

increases, it follow a non-linear pattern of amplitude dispersion, energy dissipation, bottom friction and require finer resolution grids with more node points to accurately capture the wave dynamics and minimize errors. The grid spacing should follow the Courant-Friedrich-Lewy conditions for checking the convergence of the numerical code to a certain asymptotic limit using following relationship,

$$\Delta x/\Delta t = \sqrt{(2ghmax)}$$

Where $\Delta t$ and $\Delta x$ are temporal and spatial grid sizes, hmax maximum still water depth in the computational domain, and g is the gravitational acceleration. Based on above conditions we used GEBCO bathymetry and topography data formatted into four grid of 81, 27, 9 and 3arc seconds resolutions at spacing ratio of 1:3 for grids A, B, C, and D, respectively.

The TUNAMI-N2 code uses Mansinha and Smyile's (1971) deformation model to estimate the seafloor upliftment near the source and the focal mechanism solutions and fault parameters are necessary to compute the initial deformation at the source at t=0 seconds. In addition to the grid resolution, the calibration requires earthquake source parameters (e.g., slip distribution, fault length, and width), which we adopted based on Ioualalen (2007), Rani et al. (2011), Mishra et al. (2014), and Srivastava et al. (2021) (Table 2). The five segments with different slip distributions of Sumatra earthquake (December 26, 2004) with ~1400 km rupture length (Ioualalen, 2007) are considered for modeling. We run the TUNAMI-N2 code with above input parameters to get the directivity map, wave amplitudes (run-up heights) at different tide-gauge locations in the study region.

**Table 2** Tsunamigenic earthquake deformation parameters used to simulate different scenarios a) 1881-Car Nicobar, and b) 1941-North Andaman earthquakes (Mishra et al., 2014), and c) 2004-Sumatra (Ioualalen, 2007).

| | 1881-Car Nicobar | 1941 -North Andaman | 2004 Sumatra Earthquake | | | | |
|---|---|---|---|---|---|---|---|
| Input Parameters | | | Seg1 | Seg2 | Seg3 | Seg 4 | Seg5 |
| Longitude (DD) | 92.43 | 92.5 | 94.57 | 93.90 | 93.21 | 92.60 | 92.87 |

| | | | | | | | |
|---|---|---|---|---|---|---|---|
| Latitude (DD) | 8.52 | 12.1 | 3.83 | 5.22 | 7.41 | 9.70 | 11.70 |
| Focal Depth (km) | 15 | 30 | 25 | 25 | 25 | 25 | 25 |
| Strike angle (°) | 350 | 20 | 323 | 348 | 338 | 356 | 10 |
| Rake (°) | 90 | 90 | 90 | 90 | 90 | 90 | 90 |
| Slip (m) | 5 | 5 | 18 | 23 | 12 | 12 | 12 |
| Fault Length (km) | 200 | 200 | 220 | 150 | 390 | 150 | 350 |
| Fault Width (km) | 80 | 80 | 130 | 130 | 125 | 95 | 95 |
| Dip (°) | 25 | 20 | 12 | 12 | 12 | 12 | 12 |
| Magnitude (Mw) | 7.9 | 7.7 | 9.3 | | | | |

### 3.3 Shoreline Analysis in DSAS

The USGS's digital shoreline analysis system (DSAS) version 5.1 (an ArcGIS extension) estimates shoreline changes. The procedures are executed in 4 steps: shoreline digitization, baseline generation, transect generation, and computation of the shoreline change rate (Raj et al., 2020; Natarajan et al., 2021). The digitized shorelines for 2004, 2005, and 2022 years have been added to a personal geodatabase in a single shapefile. The shoreline image data is added to the attributes as MM/DD/YYYY, and the baseline is in the meter UTM projected coordinate system. To estimate rates of change, DSAS uses baseline measurements of a time series of shorelines and a shapefile (Leatherman, 2003). Generating transects involves initially choosing a predefined set of parameters from the personal geodatabase, including settings for the baseline and shoreline. Subsequently, we placed these transects perpendicular to the shoreline, extending 800 m at intervals of 150 m along the entire shoreline, originating from the baseline. A 50 m smoothing distance was applied using the 'cast transects' tool within DSAS to ensure a smoother outcome.

The evaluation of uncertainty encompasses natural and anthropogenic forces such as wind, waves, tides, currents, and human influences, along with the accuracy of measurement techniques, including digitization, interpretation, and GPS error. The uncertainty in the

shoreline analysis is due to the influence of tides on the Landsat satellite imagery, which is minuscule in the extensive coastline of the study area. The tide gauge data of Port Blair station for 2004-2005 and 2022 are unavailable in the Permanent Service for Mean Sea Level (PSMSL) database (https://psmsl.org/data/obtaining/stations/206.php). We calculated uncertainty of 7.46m and 7.13m for 2018-2019 and 2019-2020, respectively, and the same is adopted for 2022 owing to similar ranges. To quantify uncertainty, we have adopted a confidence interval of 90% and assigned a shoreline uncertainty value of 10 meters as per the recommendations of the United States Geological Survey (USGS) under the National Assessment of Shoreline Change project (Himmelstoss et al., 2021; Den and Oele, 2018 and Joesidawati, 2016). We used End Point Rate (EPR) and Net Shoreline Movement (NSM) methods to analyze the shoreline change. The statistical mean of these parameters was computed using USGS's DSAS tool (Himmelstoss et al., 2021).

### 3.3.1 Net Shoreline Movement (NSM)

NSM is a statistical parameter used to determine the net change in the shoreline position over a specific period by finding the perpendicular distance between the most recent shoreline (in this case, 2022) and the oldest shoreline (2004) along each transect. The formula for NSM can be expressed as:

$$NSM = \{d_{2022}\text{-}d_{2004}\}m$$

### 3.3.2 End Point Rate (EPR)

EPR is a statistical parameter quantifying the shoreline change rate over time is calculated by dividing the Net Shoreline Movement (NSM) by the time elapsed between the oldest and most recent shoreline measurements, which indicates the rate of erosion or accretion. It is important to have data from at least two shoreline dates (Dolan et al., 1991; Crowell et al., 1997). The formula for EPR can be expressed as follows:

$$EPR = \left\{\frac{d2022 - d2004}{t2022 - t2004}\right\}$$

### 3.4 Land Use Land Cover Analysis (LULC)

The LULC map uses Landsat 5 TM (2004 and 2005) and Landsat 8 OLI (2022). False Colour Composite (FCC) satellite images combine near-infrared, red, and green bands to delineate five classes: Forest, built-up, Cropland, Water bodies, and Inundated areas. (Prabhbir and Kamlesh, 2011). Tone, texture, size, shape, pattern, association, and other visual interpretation techniques also were used to interpret different land use classes. Maximum likelihood is a supervised classification method used in this study to detect LULC change. Each pixel in the classified Landsat images varies over time due to changes in land cover.

## 4. Results

An analysis of the 2004 tsunamigenic earthquake's impact on the South Andaman region, focusing on tsunami directivity, arrival times, run-up heights, shoreline changes, and LULC impact, is examined in detail.

### 4.1 Tsunami studies along the South Andaman Region

We have considered three tsunamigenic seismic scenarios, namely, a) the 1881-Car Nicobar earthquake, b) the 1941-North Andaman earthquake, and c) the 2004 Sumatra earthquake, and generated the directivity and run-up model (Fig. 3). The directivity map shows that most of the energy propagation is in the East-West direction (Fig. 3 a,b,c), and the shallower waters surrounding the Andaman and Nicobar Islands has significance influence on the east-west propagation of tsunamis (Singh et al., 2012). The run-up height along the eastern coast of South Andaman is greater than the western coast (Fig. 3 b', c', d'; Table 3). This difference is due to the wider continental shelf on the Western coast of the south Andaman region and shallow water depths. In the case of a higher magnitude of tsunamigenic earthquakes in the Car Nicobar or the North Andaman region, higher run-ups will be observed along the gauge locations, which are considered for the present study (Table 3).

The arrival times of tsunamis vary from 21.75 minutes to 58 minutes across locations for these earthquakes, with the 1881-Car Nicobar earthquake generally resulting in the shortest arrival time (Fig. 3; Table 3). The run-up heights range from 1-13 m at different locations (Fig. 3; Table 3), which were influenced by earthquake magnitude, the source's proximity to observation locations, and the local coastal topography that also affected inundations. The extent of inundation, representing the area covered by the tsunami, ranges from 10m to 950m, with a wide variation across locations and earthquake events. The 2004 Andaman Sumatra earthquake resulted in higher run-up heights and inundations compared to the 1881 Car Nicobar, and 1941 Andaman earthquakes and caused extensive damage. Therefore, we considered the 2004- Andaman Sumatra earthquake for a detailed analysis of hazard assessment and scenario analysis. The arrival times (Minutes), run-up height (meter), and Inundation extent (meter) at 13 different locations along the South Andaman region by the 2004 Sumatra earthquake (Table 3) are considered for further analysis.

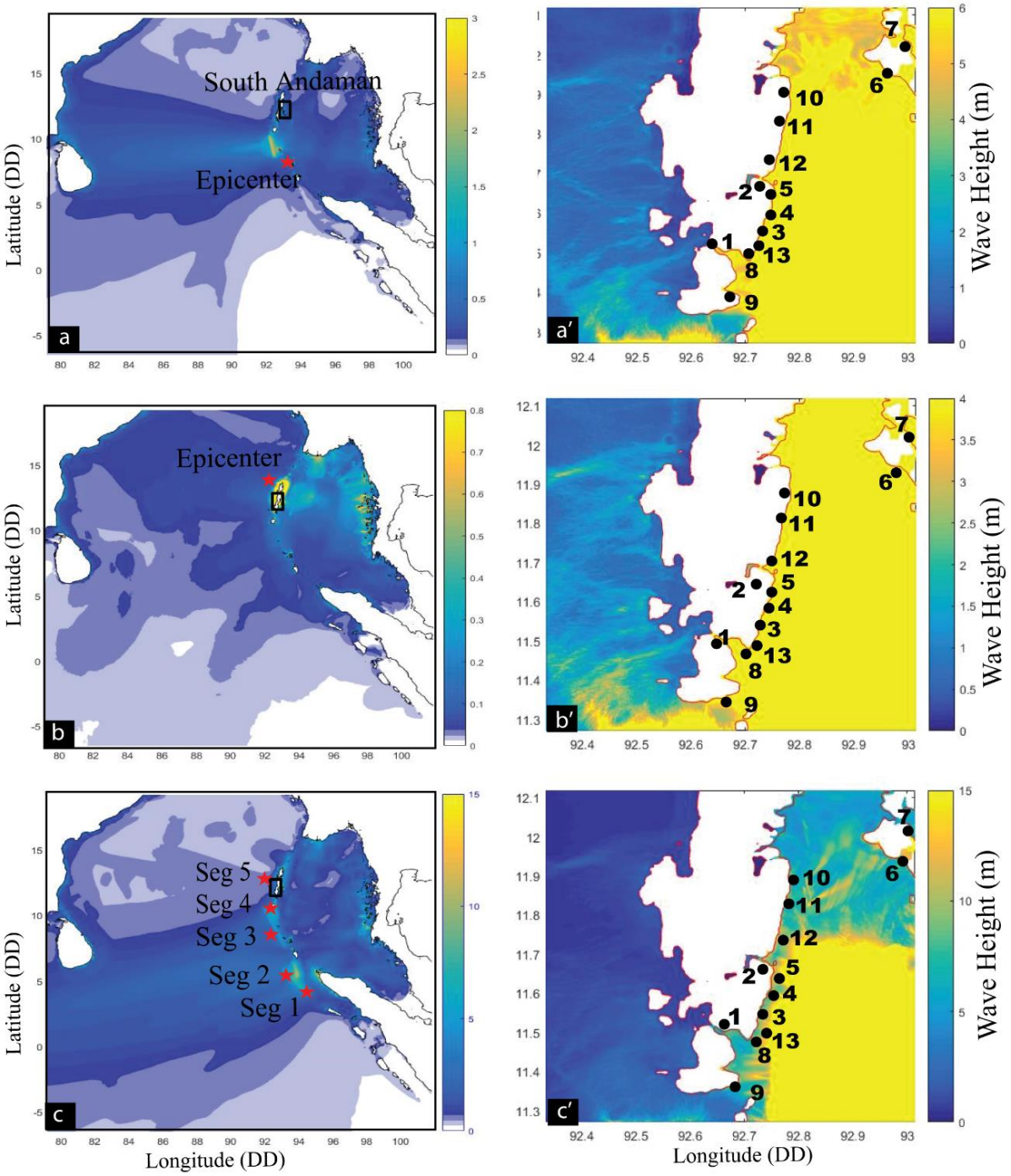


*Figure 3: (a) Directivity and (a') wave run-up height for the 1881-Car Nicobar, (**b** and **b'**) for the 1941-Andaman, and (c and c') for the 2004-Sumatra earthquakes.*

**Table 3** Estimated Arrival times, Run-up heights, and inundations at the studied locations from tsunamigenic a) 1881-Car Nicobar, b)1941-North Andaman earthquakes, and c) 2004-Sumatra earthquake sources. The SN of locations is common for Figs. 3 and 4.

| SN | Gauge Locations | Longitude Latitude (DD) | Earthquake Sources | Arrival Time(Min.) | Run-up (m) | Inundation (m) |
|---|---|---|---|---|---|---|
| 1 | Wandoorjetty | 92.614750, 11.581667 | a) 1941-North Andaman | 22.5 | 1.25 | 180 |
| | | | b) 1881 Car Nicobar | 32.80 | 2.21 | 200 |
| | | | ***c) 2004 - Sumatra*** | ***36.5*** | ***3.5*** | ***450*** |

| | | | | | | |
|---|---|---|---|---|---|---|
| 2 | Bombooflat | 92.715417, 11.700722 | a) 1941-North Andaman | 24.55 | 2.23 | 350 |
| | | | b) 1881 Car Nicobar | 31.2 | 2.35 | 650 |
| | | | ***c) 2004 - Sumatra*** | ***42*** | ***5.5*** | ***90*** |
| 3 | Corbyns Cove Beach | 92.770916, 11.642372 | a) 1941-North Andaman | 22.3 | 2.1 | 320 |
| | | | b) 1881 Car Nicobar | 28.8 | 2.3 | 580 |
| | | | ***c) 2004 - Sumatra*** | ***33*** | ***12.7*** | ***900*** |
| 4 | South Point, Port Blair | 92.702917, 11.652389 | a) 1941-North Andaman | 22 | 2.12 | 280 |
| | | | b) 1881 Car Nicobar | 28.4 | 2.31 | 500 |
| | | | ***c) 2004 - Sumatra*** | ***31.5*** | ***9.6*** | ***550*** |
| 5 | Thirupatti Temple | 92.703861, 11.581694 | a) 1941-North Andaman | 21.75 | 1.42 | 360 |
| | | | b) 1881 Car Nicobar | 46.5 | 1.65 | 400 |
| | | | ***c) 2004 - Sumatra*** | ***38*** | ***1*** | ***200*** |
| 6 | Radha Nagar | 92.951722, 11.979306 | a) 1941-North Andaman | 52 | 2.1 | 180 |
| | | | b) 1881 Car Nicobar | 54 | 3.8 | 220 |
| | | | ***c) 2004 - Sumatra*** | ***54*** | ***2.6*** | ***156*** |
| 7 | Govinda Nagar | 92.989139, 12.030167 | a) 1941-North Andaman | 56 | 1.8 | 220 |
| | | | b) 1881 Car Nicobar | 58 | 3.2 | 190 |
| | | | ***c) 2004 - Sumatra*** | ***58*** | ***3.6*** | ***195*** |
| 8 | Chidiyatopu | 92.716639, 11.499306 | a) 1941-North Andaman | 21.75 | 1.79 | 300 |
| | | | b) 1881 Car Nicobar | 26.5 | 2.05 | 500 |
| | | | ***c) 2004 - Sumatra*** | ***36*** | ***3.9*** | ***585*** |
| 9 | Rutland Island | 92.703818, 11.431497 | a) 1941-North Andaman | 25.9 | 1.01 | 585 |
| | | | b) 1881 Car Nicobar | 26.55 | 1.44 | 380 |
| | | | ***c) 2004 - Sumatra*** | ***27*** | ***6*** | ***700*** |
| 10 | Shoal Bay | 92.795963, 11.934202 | a) 1941-North Andaman | 34.8 | 1.77 | 180 |
| | | | b) 1881 Car Nicobar | 42.5 | 1.45 | 220 |
| | | | ***c) 2004 - Sumatra*** | ***56*** | ***13*** | ***950*** |
| 11 | Potatang | 92.801282, 12.027380 | a) 1941-North Andaman | 36 | 1.5 | 200 |
| | | | b) 1881 Car Nicobar | 46 | 1.4 | 180 |
| | | | ***c) 2004 - Sumatra*** | ***58*** | ***12.5*** | ***210*** |
| 12 | Madhuban Bay | 92.785534, 11.782775 | a) 1941-North Andaman | 32 | 1.9 | 180 |
| | | | b) 1881 Car Nicobar | 40 | 1.5 | 200 |
| | | | ***c) 2004 - Sumatra*** | ***54*** | ***6.9*** | ***210*** |
| 13 | Brichgunj | 92.770162, 11.618980 | a) 1941-North Andaman | 28 | 1.3 | 200 |
| | | | b) 1881 Car Nicobar | 32 | 4 | 300 |
| | | | ***c) 2004 - Sumatra*** | ***30*** | ***10*** | ***585*** |

The results show that the run-up heights range from 1 to 13 m, arrival times range from 27 to 58 min, and the inundation extent range from 90 to 950m, suggesting a significant variability in the tsunami's impact across the South Andaman Region. Due to the effects of the 2004 tsunami, the stagnation of tsunami water in the agricultural lands and low-lying areas of the Wandoor region resulted in increased soil salinity (Fig. 4a); it also damaged the bridge in

the Bombooflat area (Fig. 4b), and houses near the Sippighat area (Fig. 4c, d). Shoal Bay recorded the highest inundation extent of 950m and experienced the highest run-up height of 13m, indicating significant wave impact (Fig. 3b; Table 3). Corbyn's Cove Beach and Rutland Island experienced significant inundation distances exceeding 700m (Fig.3b, Table 3). Potatang, Corbyns Cove Beach, and Brichgunj also recorded relatively high run-up heights that exceeded 9m (Table 3). Most locations experienced arrival times between 27 and 58 minutes, indicating a relatively quick propagation of the tsunami wave. Jain et al. (2005) mentioned that tsunami waves arrived between 40 and 50 minutes in the Andaman and Nicobar Islands. Our results agree with the tsunami run-up heights estimation by Cho et al. (2008) and Prerna et al. (2015) at a few locations in the present study. South Andaman experienced significant inundations during the 2004 Sumatra earthquake, highlighting the urgent need for robust mitigation and preparedness measures in these vulnerable coastal regions. We aim to contribute to this broader goal by providing essential data and insights to support evidence-based decision-making and mitigate the adverse impacts of tsunamis on coastal populations. The study will provide workable input to the local risk management strategies involving local communities, optimizing evacuation planning, enhancing early warning systems, fortifying infrastructure resilience, and adopting a multi-hazard risk assessment approach (National Research Council, 2011).


*Figure 4: (a) Stagnation of Tsunami water in the agricultural field and Low-laying areas in Port Blair, (b) damaged bridge in Bombooflat, (c, d) damaged house in the Sippighat area near Port Blair (Photo: 01/03/2023). The number on the field photograph corresponds to respective locations as in Fig. 3.*

### 4.2 Shoreline Change during Tsunami (2004-2005) and post-tsunami (2005-2021)

The south Andaman coasts are divided into seven zones based on proximity with the inundation studies to calculate NSM and EPR to understand the short-term and long-term changes impact of coastal erosion (Fig. 5, Supplement Fig. S1-S7). The NSM and EPR are calculated over two separate time frames to comprehend the damages caused by tsunamigenic and regular wind-wave-surge events in South Andaman Island. These zones were used to understand erosion and accretion rates between (i) 2004 - 2005 (Fig. 5a) and (ii) 2005-2022 (Fig. 5b). The EPR and NSM values from 2004 to 2005 indicate the direct effect of tsunami waves, whereas 2005 to 2022 values represent periodic wind-wave-surge dynamics. Periodic coastal shoreline changes refer to the regular and repeating fluctuations in the position of the shoreline along the coast. Natural and human-induced factors can influence these changes. A total of 1,083 transects are created at 50-m intervals, distributed among the zones as follows:

Zone 1 (339 transects), Zone 2 (147 transects), Zone 3 (89 transects), Zone 4 (74 transects), Zone 5 (137 transects), Zone 6 (73 transects), and Zone 7 (220 transects). The shoreline variation rates indicate positive accretion and negative erosion (Fig. 6, Table 4). The EPR Changes in meters per year (m/y) for the periods 2004-2005 show a higher erosion rate compared to 2005-2022, particularly in Zones 3, 4, and 5 (Fig. 6a). The NSM focused on two distinct time frames, indicate the NSM rates during the tsunami, for the year of 2004-2005, and the NSM rates over the extended 17-year period from 2005 to 2022 are measured in meters (Fig. 6b). The detailed analysis of the maximum (accretion), minimum (erosion), and mean shoreline changes for each of the seven zones that occurred during the tsunami event and the post-tsunami period are discussed below.

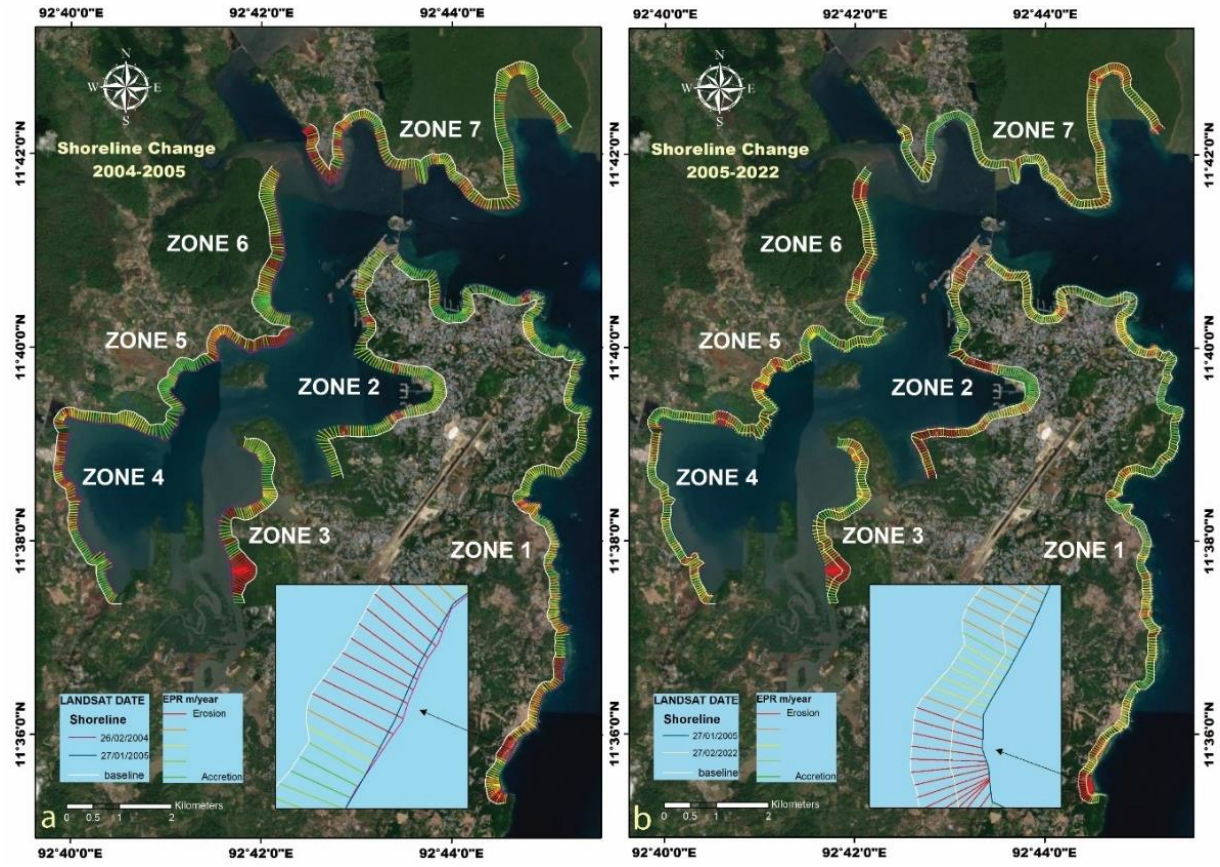


*Figure 5: Shoreline changes observed (a) during 2004-05 due to the tsunamigenic process and (b) from 2005-2022 due to wind wave surges overlaid on Google Earth images (@Google Earth). The affected coastline is subdivided into seven distinct zones for detailed analysis.*

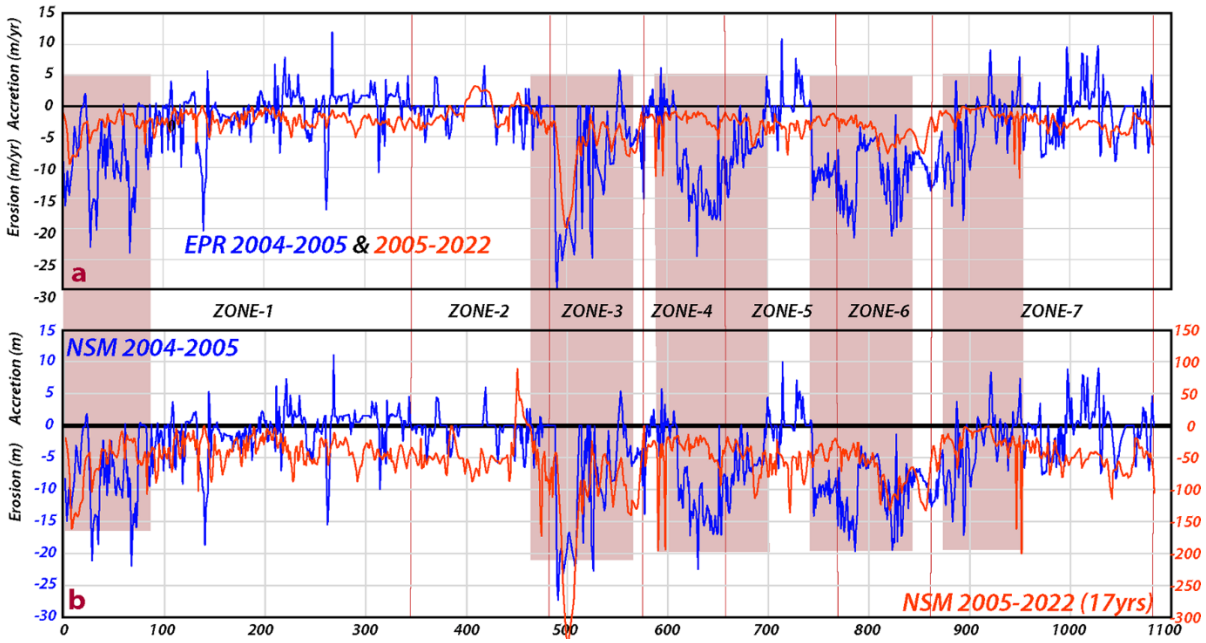


*Figure 6: (a) The rates of erosion and accretion in seven distinct Zones along the South Andaman shoreline using EPR methods, and (b) NSM have been conducted between the years 2004-2005 and 2005-2022. Highlighted color indicating high erosion zone*

**Table 4** Shoreline change in southern Andaman is observed for 2004-2005 and 2005-2022 using USGS's DSAS methods (Himmelstoss et al., 2021).

| | | 2004-2005 | | 2005-2022 | |
|---|---|---|---|---|---|
| **ZONE** | | **EPR(m/y)** | **NSM(m)** | **EPR(m/y)** | **NSM (m)** |
| **ZONE 1** | Mean | -2.85 | -2.62 | -2.55 | -43.57 |
| | Minimum | -23.9 | -21.29 | -9.44 | -161.21 |
| | Maximum | 12.05 | 11.06 | 0 | 0 |
| **ZONE 2** | Mean | -0.54 | -0.50 | -1.0639 | -18.174 |
| | Minimum | -7.17 | -6.58 | -4.56 | -77.93 |
| | Maximum | 6.54 | 6 | 3.25 | 55.56 |
| **ZONE 3** | Mean | -9.92 | -8.11 | -7.10 | -121.51 |
| | Minimum | -24.71 | -23.27 | -19.87 | -339.51 |
| | Maximum | 5.58 | 4.37 | -1.02 | -17.42 |
| **ZONE 4** | Mean | -7.92 | -7.72 | -2.24 | -38.34 |
| | Minimum | -24.47 | -22.46 | -11.42 | -195.03 |
| | Maximum | 6.23 | 5.72 | -0.79 | -13.42 |
| **ZONE 5** | Mean | -6.594 | -6.05 | -2.94 | -50.26 |
| | Minimum | -21.47 | -19.7 | -7.95 | -135.83 |
| | Maximum | 10.88 | 9.99 | -1.03 | -17.54 |
| **ZONE 6** | Mean | -9.74 | -8.94 | -4.92 | -84.05 |
| | Minimum | -21.18 | -19.44 | -7.75 | -132.39 |
| | Maximum | -1.46 | -1.34 | -1.86 | -31.73 |
| **ZONE 7** | Mean | -2.16 | -1.986 | -2.43 | -41.56 |
| | Minimum | -18.65 | -17.29 | -11.7 | -199.96 |
| | Maximum | 9.77 | 8.97 | -0.04 | -0.61 |

ZONE 1: This zone experienced a combination of erosion and accretion between 2004-05 and 2005-21. The maximum erosion rates are observed at Megapoda, with an EPR of -23.9 m/y. and -9.44 m/y., NSM analysis shows the estimated erosion is -21.29m and -161.21m respectively (Fig. S1 a, b, Table 4). The southern part of South Andaman Island has more shoreline erosion rather than accretion, which can be attributed to the heightened impact of tsunamis on the southern region, a phenomenon that is more significant when compared to the northern part of South Andaman Island. These Sediments eroded from one coastline area are often transported along the shoreline by the longshore currents. The angle of wave approach creates these currents and is responsible for moving sediment parallel to the coastline.

ZONE 2: This zone experienced a combination of erosion and accretion between 2004-05 and 2005-21. The maximum rate of erosion is -7.17 m/y and -4.56 m/y (EPR) was recorded at IOC Colony, while the maximum accretion rate of 6.54 m/y and 3.25 m/y (EPR) was observed at Ashwin Nagar Respectively. The NSM analysis indicated a shoreline retreat of -6.58 m at IOC Colony and -77.93 m advancement at Ashwin Nagar. The jetties in the Jungli Ghat port played a role in controlling erosion and accretion at these sites (Fig. S2, Table 4).

ZONE 3: This zone experienced a combination of erosion and accretion between 2004-05 and 2005-21. The maximum erosion rate is -24.71 m/y and -19.87 (EPR) at Flat Bay, while the maximum accretion rate is 5.58 m/y and (EPR) at NLC Limited. The NSM analysis revealed a shoreline retreat of -23.27 m and -339.51 m at Flat Bey. High wave energy and exposure to strong currents, which are more common near Flat Bay, can lead to increased erosion of mangrove shorelines (Fig. S3, Table 4).

ZONE 4: This zone experienced a combination of erosion and accretion between 2004-05 and 2005-21. The maximum erosion rate is -24.47 m/y at Ferrargunj and -11.24 m/y (EPR)

at PLK Creek Resort, NSM estimated erosion is -22.46 m and -195.03m at Chouldari (Fig. S4). We observed the shoreline erosion area using the Landsat time-lapse satellite images between 2004-2005, and 2022 near Flat Bay, South Andaman, has revealed noteworthy environmental changes. The dark blue color observed in 2004 and 2005 indicates the presence of deep-water bodies, whereas the light blue color in the 2022 image suggests the water bodies have become shallow with significant fresh sediment load (Fig. 7; Table 4).

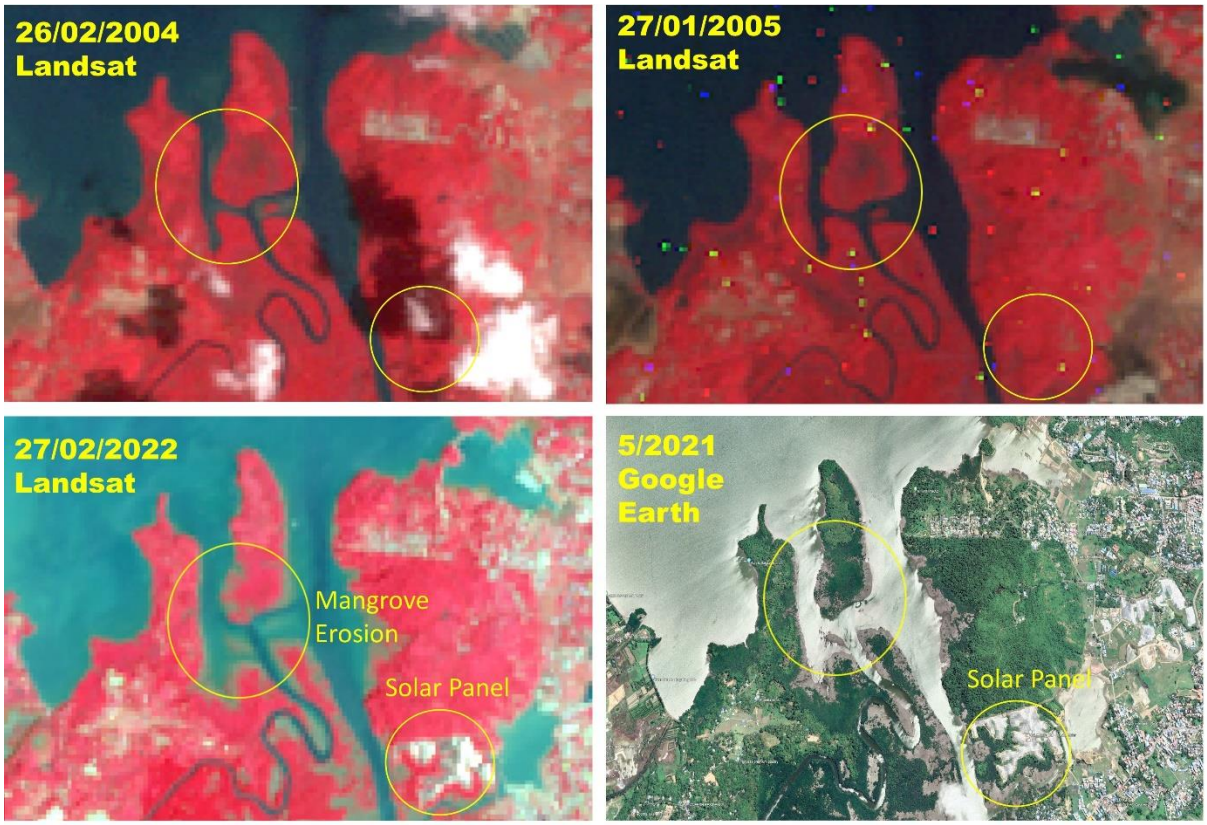


*Figure 7 shows a time-lapse satellite imagery of Landsat 8 FCC near the Flat Bay area (marked in yellow circle) during the years 2004 and 2005 showing robust mangrove coverage is evident. However, when comparing the Landsat 8 image in 2022 and the corresponding Google Earth image (@Google Earth), it is apparent that the mangrove ecosystem in this area has experienced substantial erosion and the development of Solar panels.*

ZONE 5: The maximum erosion rate of -21.47 m/y (2004-05) and -7.95 (EPR 2005-22) is recorded at Mithakhari. According to the NSM analysis, the shoreline retreated by -19.7 m and -132.39m at Mithakhari (Fig. S5). In this zone, Coastal development,

infrastructure construction, and alteration of natural hydrological patterns can disrupt sediment transport and exacerbate erosion (Fig. 8; Table 4).

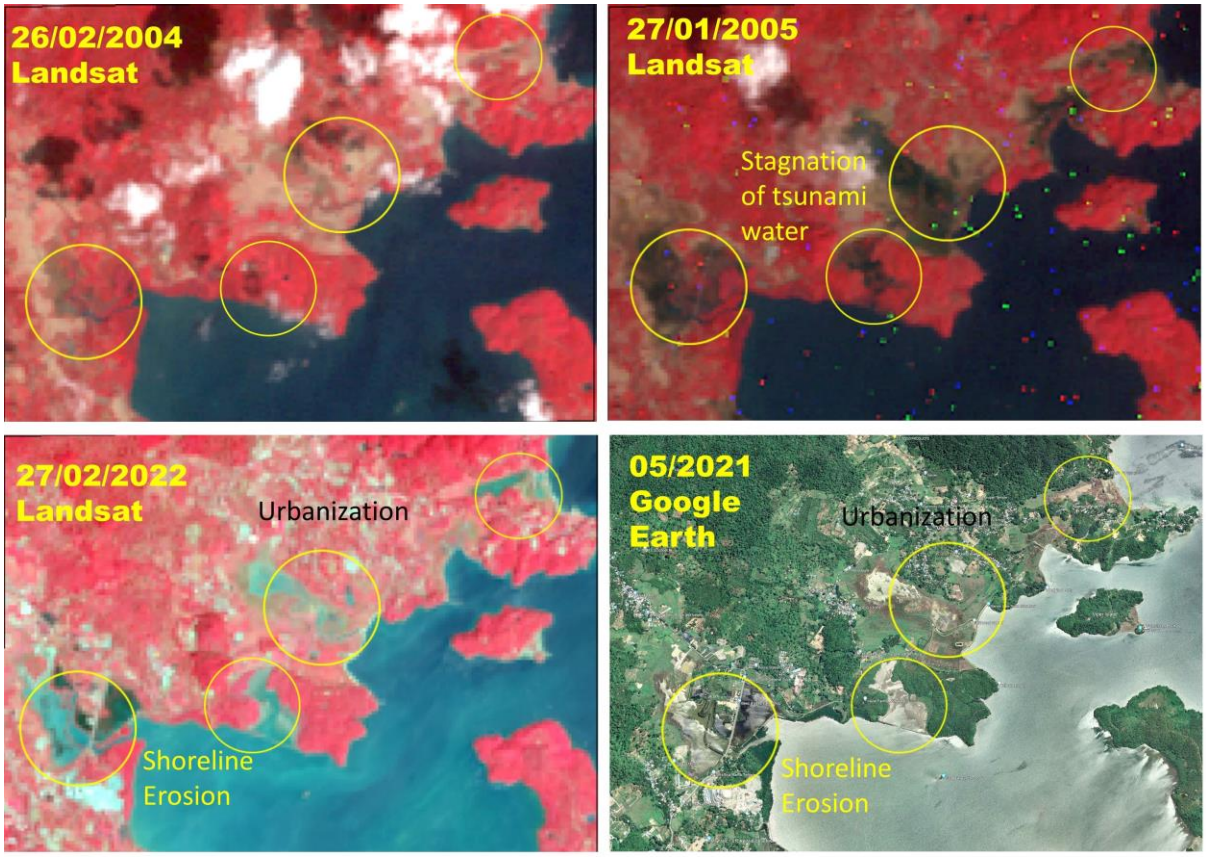


*Figure 8 shows Landsat 8 time-lapse imagery and © Google Earth imagery near the Ograbraj and Mithakhari region depicting the erosion activity during and after the tsunami and the imagery shows a significant growth in the built-up areas surrounding the tsunami-affected areas in 2004.*

ZONE 6: This zone is predominantly affected by erosion, with no observed accretion. The maximum erosion rate is -21.18 m/y and -7.75 m/y (EPR) at Namunaghar, and the NSM estimated erosion is -19.44 m and -132.39m at Namunaghar (Fig. S6). In February 2004, immediately before the catastrophic tsunami event, there was no observable presence of stagnant water in the area (Fig. 9). However, by January 2005, following the tsunami, the images distinctly exhibited the stagnant water. In February 2022, the same location exhibited substantial shoreline erosion within the extensive mangrove and agricultural area, accompanied by increased urban development along the shoreline. The progression

of urban development was also validated using Google satellite imagery. The sediment carried by ocean currents deposited in low-lying areas revealed caused shallowing and significant changes in ocean water color.

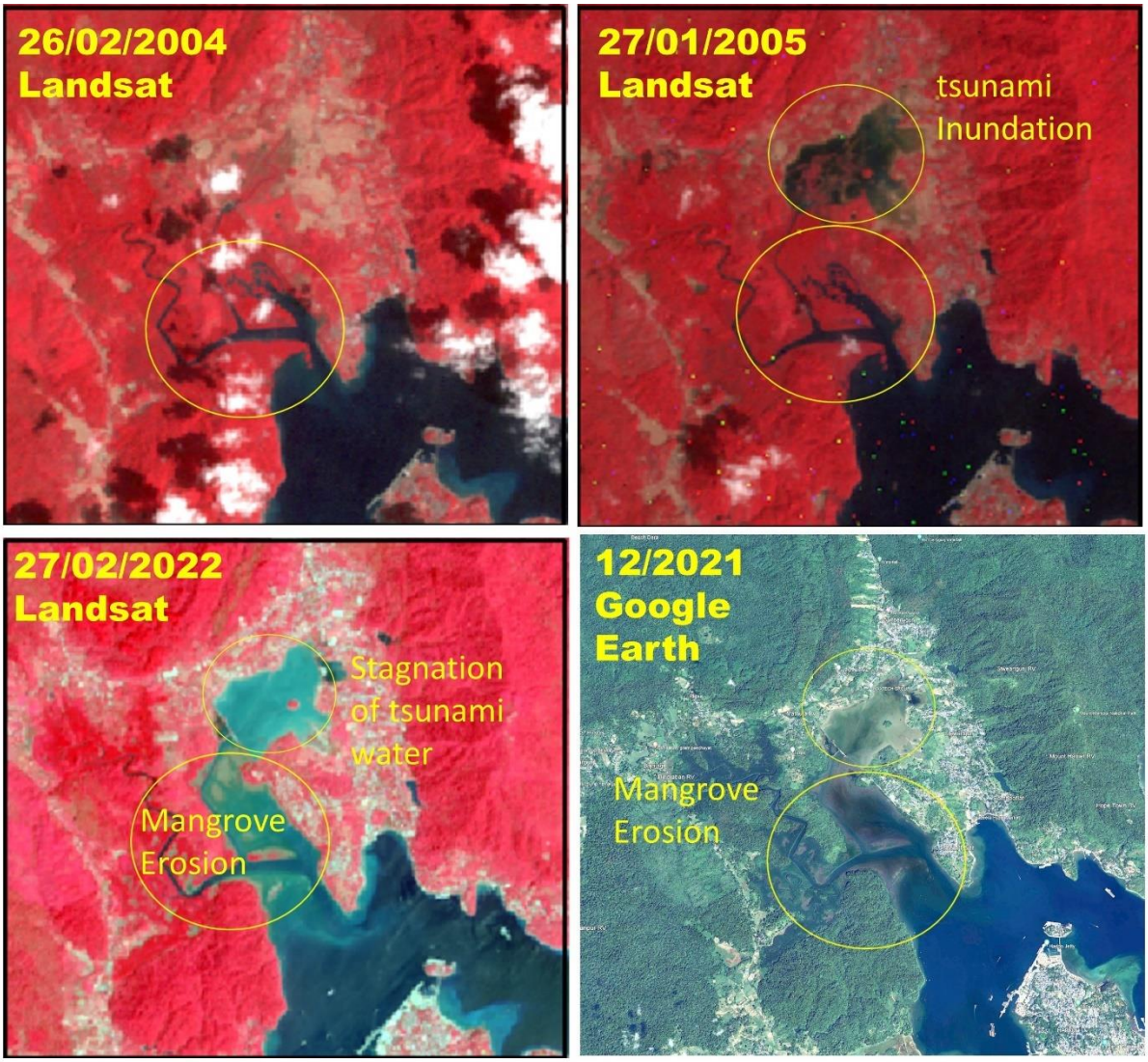


*Figure 9 shows the Change detection of the shoreline using Landsat 8 time-lapse imagery and © Google Earth imagery for 2004 before, 2005 after the tsunami, and the 2022 present status of the shoreline.*

ZONE 7: This zone experienced a combination of erosion and accretion between 2004-05 and 2005-21. The maximum erosion rate is -8.36 m/y and -11.7 m/y (EPR) at Shore Point, while the maximum accretion rate is 9.77 m/y (EPR). The NSM analysis indicated an

erosion of -17.29 m at Shore Point and -199.96 m at North Bay (Fig. S7; Table 4). Notably, a tsunami with a height of 9.6 m is observed at Shore Point.

The natural rate of shoreline movement in the South Andaman region has increased following the tsunami event, which is attributed to several factors, including the removal of vegetation cover, the softening of exposed bedrock, and the destabilization of unconsolidated materials caused by the tsunami, all of which have made the region more susceptible to erosion (Yunus et al., 2016). Comparing the erosion and accretion rates suggests the erosion rates were significantly less during the 2005-2022 period in comparison to the 2004-05 tsunami, highlighting the adverse effect of the tsunami.

### 4.3 Land Use and Land Cover (LULC) Analysis

The LULC is categorized into 5 distinct classes: Built-up, Forest, Inundation, Cropland, and water Bodies (Fig. 10). The overall accuracy obtained is 90.11%, 89.96%, and 90.30% with a quantitative assessment of $K_{hat}$ (Kappa) coefficient is 0.78, 0.762 and 0.79 for 2004,2005 and 2022 images, respectively (**Table S1**). Our primary objective is to determine the extent of land use pattern changes from 2004 to 2022 in areas affected by the 2004 tsunami. Several researchers have already examined the vulnerability and impact of the 2004 tsunami on South Andaman, including (Velmurugan et al., 2006; Debjani et al., 2012; Sachithanandam,2014).

The LULC classification for the South Andaman region in tsunami-impacted areas in the years 2004, 2005, and 2022 reveals significant changes (Fig. 10, Table 5). 1) The built-up area decreased from ~7.38% in 2004 to 6.23% in 2005, marking a 1.15% decrease. However, it subsequently increased by 11.11% by 2022. 2) Cropland coverage decreased from around 22.12% in 2004 to ~11.93% in 2005, indicating a substantial reduction of 10.19%. It then increased to 17.15% by 2022. 3) Inundation areas increased from about 3.29% in 2004 to 27.65% in 2005, showing a notable rise of 24.36%. However, by 2022, they decreased by ~18.57%. 4) Forested areas saw a significant decrease from ~66.46% in 2004 to about 51.10%

in 2005, signifying a reduction of 15.36%. This decrease persisted in 2022, remaining at ~51.10%. 5) Water bodies covered around 0.62% of the area in 2004, which increased slightly to about 0.76% in 2005. By 2022, there is a more significant increase, reaching 2.05%.

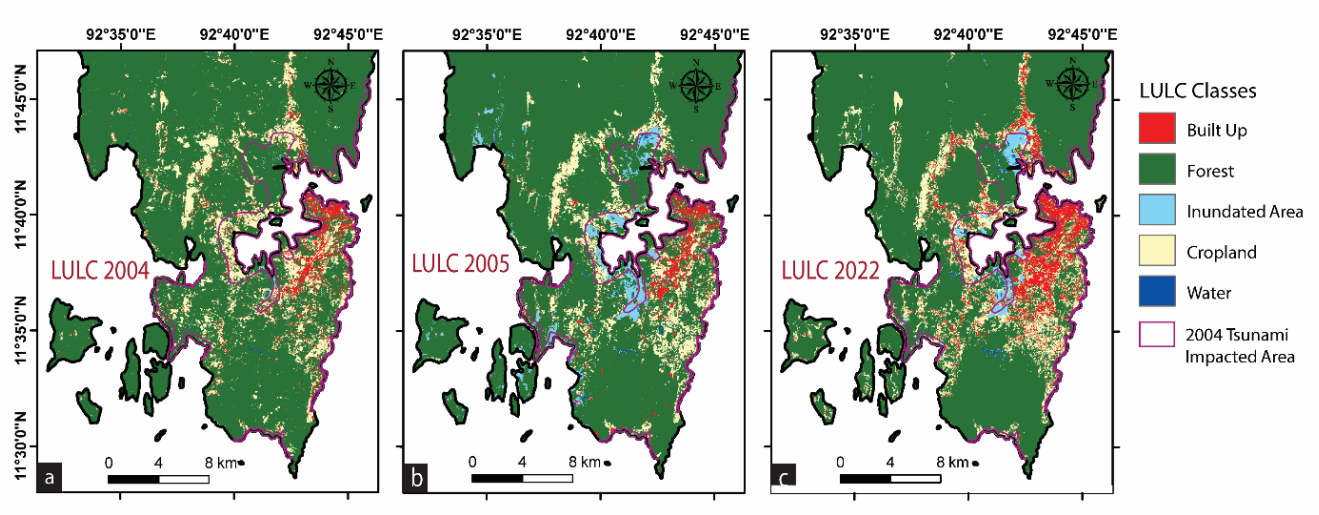


*Figure 10 (a) LULC 2004 (b) LULC 2005, and (c) LULC 2022 in tsunami-impacted areas (pink color) and South Andaman.*

**Table 5** LULC Analysis for 2004, 2005 to 2022 in tsunami impacted area

| LULC | 2004 Area in km$^2$ | 2004 % of Area | 2005 Area in km$^2$ | 2005 % of Area | 2022 Area in km$^2$ | 2022 % of area |
|---|---|---|---|---|---|---|
| Built-Up | 3.57 | 7.38 | 3.01 | 6.23 | 5.38 | 11.11 |
| Forest | 32.19 | 66.46 | 25.79 | 53.40 | 24.74 | 51.10 |
| Inundation Area | 1.64 | 3.39 | 13.36 | 27.65 | 8.99 | 18.57 |
| Cropland | 10.71 | 22.12 | 5.76 | 11.93 | 24.74 | 17.15 |
| Water Bodies | 0.30 | 0.62 | 0.36 | 0.76 | 0.99 | 2.05 |
| Total Area (Sq. Km) | 48 | 100 | 48 | 100 | 48 | 100 |

The LULC classification for the South Andaman region in the years 2004, 2005, and 2022 shows significant changes (Figure 10, Table 6)

**1) Built-Up Area**: In 2004, the built-up area covered 19.92 km², constituting ~3.84% of the total study area. By 2005, this area had reduced to 17.66 km², accounting for 3.41% of

the total area. by 2022, there was a significant expansion, with the built-up area occupying 45.07 km², representing 8.68% of the total region.

**2) Forest**: In 2004, forests dominated the landscape, covering 432.85 km², which was approximately 83.43% of the total study area. By 2005, this forested area slightly decreased to 420.79 km², comprising 81.27% of the total area. However, by 2022, the forest cover continued to decline, with an area of 408.66 km², accounting for 78.78% of the total region.

**3) Inundation Area**: In 2004, the inundation area was limited, covering 3.40 km² or 0.65% of the total area. In 2005, there was a substantial increase, expanding to 28.41 km², which represented 5.48% of the total area. By 2022, the inundation area decreased to 13.89 km², making up 2.66% of the total region.

**4) Cropland**: Cropland covered 61.77 km² in 2004, accounting for 11.90% of the total study area. By 2005, this area reduced to 49.34 km², representing 9.53% of the total area. In 2022, the cropland area further decreased to 48.65 km², making up 9.37% of the total region.

**5) Water Bodies**: In 2004, water bodies covered a small area of 0.83 km², approximately 0.16% of the total area. By 2005, this area slightly increased to 1.54 km², constituting 0.29% of the total region. There was a more significant expansion during 2022, with water bodies occupying 2.45 km², accounting for 0.47% of the total area.

**Table 6** LULC Analysis for 2004, 2005 to 2022 in the Study region

| LULC | 2004 Area in $km^2$ | 2004 % of Area | 2005 Area in $km^2$ | 2005 % of Area | 2022 Area in $km^2$ | 2022 % of area |
|---|---|---|---|---|---|---|
| Built-Up | 19.92 | 3.84 | 17.66 | 3.41 | 45.07 | 8.68 |
| Forest | 432.85 | 83.43 | 420.79 | 81.27 | 408.66 | 78.78 |
| Inundation Area | 3.40 | 0.65 | 28.41 | 5.48 | 13.89 | 2.66 |
| Cropland | 61.77 | 11.90 | 49.34 | 9.53 | 48.65 | 9.37 |
| Water Bodies | 0.83 | 0.16 | 1.54 | 0.29 | 2.45 | 0.47 |

| | | | | | | |
|---|---|---|---|---|---|---|
| Total Area (Sq. Km) | 518 | 100 | 518 | 100 | 518 | 100 |

## 5. Discussion

The complex interaction between geomorphology, shoreline change, LULC changes, and economic factors in tsunami vulnerability and impact assessment in South Andaman is discussed below;

### 5.1 Shoreline changes VS LULC

The impact of tsunamis varies due to differences in landforms, relief, slope, elevation, and the presence (or absence) of natural barriers such as coral reefs and mangroves. It has been observed that for a given water depth on the shelf, if the continental slope is steeper, greater mangrove cover, greater relief, and higher elevation can result in a greater amount of energy being reflected, leading to a smaller tsunami wave height on the shelf. On the other hand, with a flatter slope, low relief, and less vegetation cover area on the coastal side, the reduced reflection and effect of shoaling can increase tsunami wave height (Siva et al., 2016). Coastal erosion is a natural process in south Andaman that occurs when waves, currents, tsunamis, and tides erode the shoreline, removing sediment and land over time. Factors such as sea-level rise, wave energy, storm events, and human activities can contribute to increased rates of erosion.

Over time, the geomorphological landforms continue to shape and modify the landscape. However, human activities and developmental pressures are significant drivers of LULC change in South Andaman (Fig. 10 a, b, c). Common LULC changes observed in the area include deforestation for urban expansion, conversion of land for agriculture, infrastructure development, and alterations to the coastal zone (Yuvaraj et al., 2014; Thakur et al., 2017; Jaman et al., 2022). The interaction between geomorphology and LULC change is particularly evident in the coastal regions of South Andaman, where coastal erosion and accretion processes influence both LULC patterns and development decisions. The erosion occurring near the

shoreline leads to the loss of valuable land, affecting agricultural areas and forest regions (Fig. 7,8,9). Conversely, accretion processes can contribute to the growth of coastal areas by building new landforms and influencing land use decisions in those locations (Nagabhatla et al., 2006; Ali and Narayana, 2015; Mageswaran et al., 2021).

### 5.2 Inundation and run observation

Our computations have shown that the tsunami wave heights for around 5.5 m inundation 90 m are observed in Bombooflat (Fig.4b). Similarly, the harbor area of Port Blair has seen structural failures in some building's foundations, and our computations show wave heights of 3.6m in that area. Chidiya Tapu, which is 25 km from Port Blair, the estimated run-up is 3.9 m, and the inundation is 585 m, which shows a gradual slope in the region (Fig. 2). Coming to the Southpoint Magar area (Port Blair), a high run-up of 8.5 m is computed, and the inundation level is 550 m. Houses located near the open sea were completely washed away. At Wandoor Jetty in Port Blair, the calculated run-up is 3.46, the inundation is 450m, and the saltwater intrusion was observed due to the tsunami.

### 5.3 LULC vs economic change:

The presence of people, infrastructure, or assets in a hazard-prone location is referred to as exposure, and vulnerability is the degree to which a person, community, or system is susceptible to the impacts of a hazard. Vulnerability is determined by physical, social, economic, and environmental factors. (United Nations Office for Disaster Risk Reduction). Several factors can contribute to changes in exposure, such as population growth, Industrial development, and LULC change. It is anticipated that the population of the Andaman and Nicobar Islands will double by 2050 (Nanda and Haub, 2007), and the islands are experiencing an increasing influx of tourists. The increased population density in these regions intensifies the strain on already vulnerable lands. As a result, when a disaster, such as a natural calamity,

488 occurs in these areas, it affects the tourists and has severe repercussions for the large local
489 population heavily dependent on tourism-related activities (Annan et al., 2005; Wood et al.,
490 2019; Sathiparan et al., 2020, Hamuna et al., 2019). The increases in population from 1971 to
491 2020, as well as built-up areas, are shown before and after the 2004 tsunami, and GSDP from
492 2001 to 2020 in tsunami-prone areas of South Andaman are observed in Fig. 11.

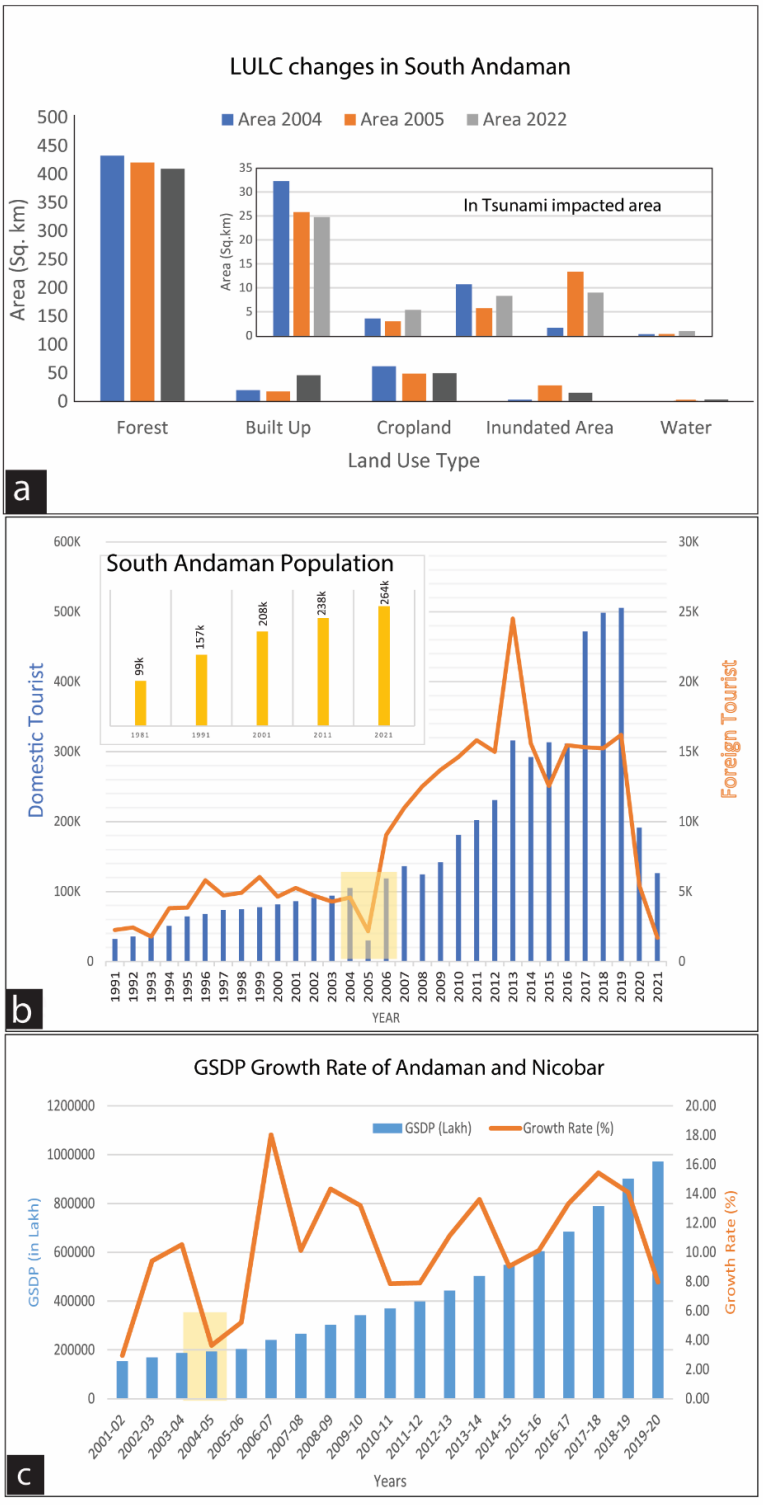


493

494 *Figure 11 (a) LULC change in south Andaman and also in tsunami-affected areas of 2004. The LULC classification*
495 *reveals that there has been a significant increase in built-up areas, inundated areas, and water bodies, while the*
496 *agricultural land and vegetation have decreased. The increasing trends of tourists and local population in south*
497 *Andaman can be seen in Fig. (b). The GSDP growth rate shows the macroeconomic impact on GSDP in 2005 due*
498 *to the tsunami impact (c).*

The increase in built-up areas could also positively impact the GSDP by boosting the construction and real estate sectors and providing more job opportunities in the tourism and hospitality industries (Fig. 11a). The 2004 Indian Ocean tsunami significantly impacted the GSDP of the Andaman and Nicobar Islands, particularly in the tourism and fisheries industries (Fig 11c). According to a report by the National Institute of Disaster Management, the Andaman and Nicobar Islands suffered losses amounting to INR 7.5 billion due to the 2004 tsunami, with damages to the tourism industry being the most significant. It is important to carefully manage this growth and ensure sustainable development practices protecting both the natural environment and the local population's well-being. This includes implementing effective disaster preparedness measures, promoting sustainable tourism practices, and balancing economic development with environmental conservation in the region.

### 5.4 Implication for changing scenario of vulnerability

India Inc. estimates that the total losses surpassed Rs 3,000 crore. Specifically, the losses in Andaman & and Nicobar Islands exceeded Rs 1,000 crore as per industry estimates (Economictimes.com). If a tsunami of similar magnitude were to occur again, the economic loss would be five times as high as those experienced in 2004. After the 2004 tsunami, the coastal area experienced significant development, with built-up areas expanding in already affected areas from ~7.38 % in 2004 to ~11.11 % in 2022. This increase in urbanization and infrastructure means that more properties, businesses, and critical facilities are now located in the coastal zone. The affected region's local population grew from 208k in 2001 to 264k in 2021 (Figure 11b). With more people living in the coastal area, there is a higher risk of casualties and a greater demand for resources and aid during and after a tsunami. The number of tourists visiting the coastal area has increased significantly, from 98,000 tourists in 2001 to 500,000 by 2019 (Figure 11b). Tourists are generally less familiar with local hazards and evacuation routes, making them more vulnerable during a tsunami. The presence of a large

number of tourists can add complexity to evacuation and relief efforts, potentially leading to higher economic losses. The region has experienced a sharp decline in forest and cropland areas. Forests act as natural buffers, helping to reduce the impact of a tsunami by absorbing some of the wave energy. Additionally, the loss of cropland can disrupt the supply chain during and after a disaster, affecting food availability and leading to economic losses beyond property damage.

## 6. Conclusions

The South Andaman region is vulnerable to tsunamis due to its location in the seismically active zone. In such an environment, tsunami preparedness and resilience are crucial. This includes implementing effective early warning systems, raising public awareness, and strengthening infrastructure resilience. Incorporating ecosystem-based approaches, such as preserving and restoring natural coastal land, can also contribute to reducing tsunami vulnerability. The South Andaman region is prone to shoreline changes due to natural processes and human activities. Regular monitoring and assessing these changes is crucial to understanding their impacts on coastal ecosystems and communities. Implementing appropriate coastal management strategies, such as beach nourishment, dune restoration, and erosion control measures, can help mitigate the negative effects of shoreline changes. It is important to adopt sustainable land use practices that balance economic development with resource conservation and responsible use. This involves promoting eco-friendly tourism, protecting sensitive ecosystems like mangroves and coral reefs, and implementing land use planning that considers the carrying capacity and vulnerability of the region. Tsunami modeling along the coastal locations shall help decision-makers how to construct structures along the coast. Decision makers will also be able to quantify the tsunami impact on sloping beaches, Flat beaches, and areas having boulders/mangroves. Engaging local communities, stakeholders, and indigenous knowledge holders in decision-making processes and promoting

549 capacity-building initiatives are critical for ensuring the sustainable development of the
550 Andaman region.

551 **Code availability**

552 No

553 **Data availability**

554 All data included in this study are available upon request by contacting the corresponding
555 author**.**

556 **Authors' contributions**

557 Vikas Ghadamode: Computations, Fieldwork, and Manuscript Writing.

558 K. Kumari Aruna: TUNAMI-N2 Computation and Fieldwork, Manuscript Writing

559 Anand Kumar Pandey: Manuscript Editing and Contribute Ideas and Suggestions

560 Kirti Srivastava: Paper Writing and TUNAMI-N2 Computations

561 **Competing interests / Conflicts of interest/**

562 The authors declare that they have no known conflicts of interest.

563 **Declarations**

564 The authors declare that they have no known conflicts of interest.

565 **Financial support**

566 No Funding

567 **Acknowledgements:**

568 The authors acknowledge encouragement and permission to publish from the Director, CSIR-
569 NGRI (Ref. No. NGRI/Lib/2024/Pub-51). VG acknowledges UGC, India, for SRF for
570 pursuing a PhD (Grant no.: 10/UGC-JRF/209/19-ESTT).

571

## References


Ali, P. Y., & Narayana, A. C.: Short-term morphological and shoreline changes at Trinkat Island, Andaman and Nicobar, India, after the 2004 tsunami. Marine Geodesy,38(1), 26-39, https://doi.org/10.1080/01490419.2014.908795 , 2015.

Annan, K.: Reducing Risks from Tsunamis: Disaster and Development. Nueva York: UNDP, 2005.

Bandopadhyay, P. C., & Carter, A.: Chapter 2 Introduction to the geography and geomorphology of the Andaman–Nicobar Islands. Geological Society, London, Memoirs, 47(1), 9-18, https://doi.org/10.1144/M47.2, 2017.

Bhat, G.R., Balaji, S. & Yousuf, M.: Tectonic geomorphology and seismic hazard of the east boundary thrust in northern segment of the Sunda–Andaman subduction zone. Nat Hazards 116, 401–423, https://doi.org/10.1007/s11069-022-05680-6, 2023.

Boak EH, Turner IL.: Shoreline definition and detection: a review. J Coast Res 21:688–703, https://doi.org/10.2112/03-0071.1, 2005.

Cho, Y. S., Lakshumanan, C., Choi, B. H., & Ha, T. M.: Observations of run-up and inundation levels from the teletsunami in the Andaman and Nicobar Islands: A field report. Journal of Coastal Research, 24(1), 216-223, https://doi.org/10.2112/06-0662.1, 2008.

Cooper JA, Jackson D, Nava F, McKenna J, Malvarez G.: Storm impacts on an embayed high energy coastline, western Ireland. Marine Geol 210:261–280, https://doi.org/10.1016/j.margeo.2004.05.012, 2004.

Crowell, M., Douglas, B. C., & Leatherman, S. P.: On forecasting future US shoreline positions: a test of algorithms. Journal of Coastal Research, 1245-1255, http://www.jstor.org/stable/4298734, 1997.

Curray, J. R.: Tectonics and history of the Andaman Sea region. Journal of Asian Earth Sciences, 25(1), 187-232, https://doi.org/10.1016/j.jseaes.2004.09.001, 2005.

Davis, R.A.:Human Impact on Coasts. In: Finkl, C.W., Makowski, C. (eds) Encyclopedia of Coastal Science. Encyclopedia of Earth Sciences Series. Springer, Cham, https://doi.org/10.1007/978-3-319-93806-6_175, 2019.

Den Boer, E. L., & Oele, A. C.: Determination of shoreline change along the East-Java coast, using the Digital Shoreline Analysis System. In MATEC Web of Conferences (Vol. 177, p. 01022). EDP Sciences, https://doi.org/10.1051/matecconf/201817701022, 2018.

Devi, E. U., & Shenoi, S. S. C.: Tsunami and the effects on coastal morphology and ecosystems: a report. Proceedings of the Indian National Science Academy, 78(3), 513-521, 2012.

Dolan, R., Fenster, M. S., & Holme, S. J.: Temporal analysis of shoreline recession and accretion. Journal of coastal research, 723-744, http://www.jstor.org/stable/4297888, 1991.

Ghadamode, V., Srivastava, K., Singh, R. K., & Pandey, A. K.: Spatial analysis techniques for tsunami vulnerability and inundation mapping of Andaman region using remote sensing, GIS, AHP, and Fuzzy logic methods. Environmental Earth Sciences, 81(17), 427, https://doi.org/10.1007/s12665-022-10548-w, 2022.

Ghosh, T., Jana, P., Giritharan, S., Bardhan, S., Basir, S. R., & Roy, A. G.:Tsunami Survey in Andaman Nicobar Group of Islands. *Sumatra–Andaman Earthquake and Tsunami*, *26*, 2004.

612 Hamuna, B., Kalor, J. D., & Tablaseray, V. E.: The impact of tsunami on mangrove spatial change in
613 the eastern coast of Biak Island, Indonesia. Journal of Ecological Engineering, 20(3),
614 http://dx.doi.org/10.12911/22998993/95094, 2019.

615 Himmelstoss, E., Henderson, R. E., Kratzmann, M. G., & Farris, A. S.: Digital shoreline analysis system
616 (DSAS) version 5.1 user guide (No. 2021-1091). US Geological Survey,
617 https://doi.org/10.3133/ofr20211091, 2021.

618 Imamura, F.: Review of Tsunami Simulation with a Finite Difference Method. Long Waves Runup
619 Models, 1996.

620 Imamura, F., & Imteaz, M. A.: Long waves in two-layers: governing equations and numerical model.
621 Science of Tsunami Hazards, 13(1), 3-24,1995.

622 Jain, S. K., Murty, C. V. R., Rai, D. C., Malik, J. N., Sheth, A., & Jaiswal, A.: Effects of M9 Sumatra
623 earthquake and tsunami of December 26, 2004. Current Science, 88(3), 357-359,
624 https://www.currentscience.ac.in/Volumes/88/03/0357.pdf, 2005.

625 Jaman, T., Dharanirajan, K., & Rana, S.: Land use and Land cover Change detection and Its
626 Environmental Impact on South Andaman Island, India using Kappa coefficient Statistical
627 Analysis and Geospatial Techniques, 2022.

628 Jayakumar K, Malarvannan S.: Assessment of shoreline changes over the Northern Tamil Nadu Coast,
629 South India using WebGIS techniques. J Coast Conserv. 20(6):477–487,
630 https://link.springer.com/article/10.1007/s11852-016-0461-9, 2016.

631 Jevrejeva, S., Jackson, L., Riva, R., Grinsted, A., & Moore, J.: Sea level rise with warming above 2
632 degree. In EGU General Assembly Conference Abstracts (p. 3637), 2017.

633 Joesidawati, M. I.: Shoreline change in Tuban district, East Java using geospatial and digital shoreline
634 analysis system (DSAS) techniques. International Journal of Oceans and Oceanography, 10(2),
635 235-246, 2016.

636 Kumar ST, Mahendra RS, Nayak S, Radhakrishnan K, Sahu KC.: Coastal vulnerability assessment for
637 Odisha state, East coast of India. J Coast Res 26:523–534, https://doi.org/10.2112/09-1186.1,
638 2010.

639 Kumari P, Jnaneswari K, Rao D, Sridhar D.: Application of remote sensing and geographical
640 information system techniques on geomorphological mapping of coastal part of East Godavari
641 district. Andhra Pradesh, India. Int J Eng Sci Tech 4:4296–4300,
642 https://link.springer.com/article/10.1007/s11069-016-2252, 2012.

643 Leatherman, S. P.: Shoreline change mapping and management along the US East Coast. Journal of
644 Coastal Research, 5-13, 2003.

645 Mageswaran, T., Sachithanandam, V., Sridhar, R., Mahapatra, M., Purvaja, R., & Ramesh, R.: Impact
646 of sea level rise and shoreline changes in the tropical island ecosystem of Andaman and Nicobar
647 region, India. Natural Hazards, 109, 1717-1741,
648 https://link.springer.com/article/10.1007/s11069-021-04895-3, 2021.

649 Mansinha, L., and Smylie, D.E.: The displacements fields of inclined faults, Bull. Seismol. Soci. Am.,
650 61(5), 1433-1440, 1971.

651 Mishra, P., Usha, T., & Ramanamurthy, M. V.: Evaluation of tsunami vulnerability along the northeast
652 coast of India. Continental Shelf Research, 79, 16-22, 2014.

Misra, A., & Balaji, R.: A study on the shoreline changes and Land-use/land-cover along the South Gujarat coastline. Procedia Engineering, 116, 381-389, https://doi.org/10.1016/j.proeng.2015.08.311, 2015.

Moran CAA.: Spatio-temporal analysis of texas shoreline changes using GIS technique. Mediterranean Mar Sci 2:5–13, https://hdl.handle.net/1969.1/408, 2003.

Mukhopadhyay, A., Mukherjee, S., Hazra, S., & Mitra, D.:Sea level rise and shoreline changes: a geoinformatic appraisal of Chandipur coast, Orissa. *Int J Geol Earth Environ Sci*, *1*(1), 9-17, 2011.

Murali M, Ankitha M, Amritha S, Vethamony P.: Coastal vulnerability of Puducherry coast, India, using analytical hierarchical process. Nat Hazards Earth Syst Sci 13:3291–3311, https://doi.org/10.5194/nhess-13-3291-2013, 2013, 2013.

Nagabhatla, N., Roy, P. S., & Jagdale, R.: Evaluating the change (1968-2001) in landscape pattern and analyzing disturbance in Baratang Forest Division (Andaman Islands), SOUTHEAST ASIA, https://hdl.handle.net/10568/40948, 2006.

Nanda, A. R., & Haub, C.: The future population of India–a long-range demographic view. Popul Res Bureau, 2007.

Natarajan, L., Sivagnanam, N., Usha, T., Chokkalingam, L., Sundar, S., Gowrappan, M., & Roy, P. D.: Shoreline changes over last five decades and predictions for 2030 and 2040: a case study from Cuddalore, southeast coast of India. *Earth Science Informatics*, *14*(3), 1315-1325, 2021.

National Research Council: Tsunami warning and preparedness: an assessment of the US tsunami program and the nation's preparedness efforts, Committee on the Review of the Tsunami Warning and Forecast System and Overview of the Nation's Tsunami Preparedness, National Research Council, 284 pp, 2011.

Nayak S.: Use of coastal data in coastal mapping. Indian Carto CMMC 147–156, 2002.

Raj, N., Rejin Nishkalank, R.A., Chrisben Sam, S.: Coastal Shoreline Changes in Chennai: Environment Impacts and Control Strategies of Southeast Coast, Tamil Nadu. In: Hussain, C. (eds) Handbook of Environmental Materials Management. Springer, Cham. https://doi.org/10.1007/978-3-319-58538-3_223-1, 2020.

Prabhbir Singh., and Kamlesh Khanduri.: Land use and Land cover change detection through Remote Sensing & GIS Technology: Case study of Pathankot and Dhar Kalan Tehsils. Inter. Journal, of. Geomatics and Geosciences 1(4), pp 839-846, 2011.

Prerna, R., Srinivasa Kumar, T., Mahendra, R. S., & Mohanty, P. C.: Assessment of Tsunami Hazard Vulnerability along the coastal environs of Andaman Islands. Natural Hazards, 75, 701-726, https://link.springer.com/article/10.1007/s11069-014-1336-8, 2015.

Ramalanjaona, G.: Impact of 2004 tsunami in the islands of Indian Ocean: Lessons learned. Emergency Medicine International, https://doi.org/10.1155/2011/920813, 2011.

Rani, V. S., Srivastava, K., & Dimri, V. P.: Tsunami propagation and inundation due to tsunamigenic earthquakes in the Sumatra-Andaman subduction zone: Impact at Visakhapatnam. Marine Geodesy, 34(1), 48-58. https://doi.org/10.1080/01490419.2011.547802, 2011.

Reguero, B. G., Beck, M. W., Agostini, V. N., Kramer, P., & Hancock, B., Coral reefs for coastal protection: A new methodological approach and engineering case study in Grenada. Journal of

694 Environmental Management, 210, 146-161, https://doi.org/10.1016/j.jenvman.2018.01.024,
695 2018.

696 Rowland, E. D., Lolade, A. A., Nicholas, D. O., Opukumo, A. W., & Omonefe, F.: The Environmental
697 Impact of Shoreline Changes and Land Use/Land Cover Change Detection in the Niger Delta
698 Region using Geospatial Technology. Journal of Asian Scientific Research, 12(4), 237-248,
699 2022.

700 Sachithanandam, V., Mageswaran, T., Ragavan, P., Mahapatra, M., Sridhar, R., Ramesh, R., & Mohan,
701 P. M.: Mangrove regeneration in tsunami-affected area of north and south Andaman using insitu
702 and remote sensing techniques, 2014.

703 Sarkar, D., Mukhopadhyay, A., & Hazra, S.: Nature of tsunami and paleo tsunami deposits of South
704 Andaman. Int J Basic Appl Sci Res, 2(3), 2275-2285, 2012.

705 Sathiparan, N.: An assessment of building vulnerability to a tsunami in the Galle coastal area, Sri Lanka.
706 Journal of Building Engineering, 27, 100952, https://doi.org/10.1016/j.jobe.2019.100952,
707 2020.

708 Scheffers A, Scheffers S, Kelletat D.: Paleotsunami relics on the southern and central Antillean island
709 arc. J Coast Res 21:263–273, https://doi.org/10.2112/03-0144.1, 2005.

710 Shaw, G., & Williams, A.: Impact of the Tsunami on the Tourism Industry and Ecosystem of the
711 Andaman and Nicobar Islands, India,2006.

712 Sheth, A., Sanyal, S., Jaiswal, A., & Gandhi, P.: Effects of the December 2004 Indian Ocean tsunami
713 on the Indian mainland. Earthquake spectra, 22(3_suppl), 435-473,
714 https://doi.org/10.1193/1.2208562, 2006.

715 Singh, A. P., Murty, T. S., Rastogi, B. K., & Yadav, R. B. S.: Earthquake generated tsunami in the
716 Indian Ocean and probable vulnerability assessment for the east coast of India. Marine Geodesy,
717 35(1), 49-65, https://doi.org/10.1080/01490419.2011.637849,2012.

718 Siva M.: Behera MR. Effect of continental slope on N-wave type tsunami run-up. The International
719 Journal of Ocean and Climate Systems, https://doi.org/10.1177/1759313116656865, 2016.

720 South Andaman District – Population.: **https://www.census2011.co.in/census/district/53-south-**
721 **andaman.html**, 2011-2023.

722 Srivastava, K., Begum, F., & Jakkula, M.: Tsunami Modelling and Run-ups along Indian Coasts.
723 Journal of the Geological Society of India, 97, 1307-1312, https://doi.org/10.1007/s12594-021-
724 1861-5, 2021.

725 Sudha Rani NNV, Satyanarayana ANV, Bhaskaran PK.: Coastal vulnerability assessment studies over
726 India: a review. Nat Hazards, https://link.springer.com/article/10.1007/s11069-015-1597,
727 2015.

728 Thakur, S., Dharanirajan, K., Ghosh, P. B., Das, P., & De, T. K.: Influence of anthropogenic activities
729 on the land use pattern of South Andaman Islands. Research Journal of Marine Sciences, 5(1), 1-
730 10, 2017.

731 The Economic Times: https://economictimes.indiatimes.com/tsunami-hits-india-inc-with-rs-3000-cr-
732 loss/articleshow/974281.cms?from=mdr

733 Thieler ER, Himmelstoss EA, Zichichi JL, Ergul A.: Digital shoreline analysis system (DSAS) version
734 4.0-an ArcGIS extension for calculating shoreline change. US Geological Survey open-file report
735 2008–1278. US Geological Survey, Woods Hole, https://doi.org/10.3133/ofr20081278, 2009.

736 Thiéblemont, R., Le Cozannet, G., Rohmer, J., Toimil, A., Álvarez-Cuesta, M., and Losada, I. J.: Deep
737 uncertainties in shoreline change projections: an extra-probabilistic approach applied to sandy
738 beaches, Nat. Hazards Earth Syst. Sci., 21, 2257–2276, https://doi.org/10.5194/nhess-21-2257-
739 2021, 2021

740 Tonisso H, Suursarr U, Kont A.: Maps, aerial photographs, orthophotos, and GPS data as a source of
741 information to determine shoreline changes, coastal geomorphic processes and their relation to
742 hydrodynamic conditions on Osmussa island, The Baltic sea. IGRSS 12:987–1159,
743 https://doi.org/10.1109/IGARSS.2012.6350382, 2012.

744 Velmurugan, A., Swarnam, T. P., & Ravisankar, N.: Assessment of tsunami impact in South Andaman
745 using remote sensing and GIS. J. Indian Soc. Remote Sensing, 34(2), 193-202, 2006.

746 Wood, N., Jones, J. M., Yamazaki, Y., Cheung, K. F., Brown, J., Jones, J. L., & Abdollahian, N.:
747 Population vulnerability to tsunami hazards informed by previous and projected disasters: a case
748 study of American Samoa. Natural Hazards, 95, 505-528,
749 https://link.springer.com/article/10.1007/s11069-018-3493-7, 2019.

750 United Nations Office for Disaster Risk Reduction (UNDRR):
751 https://www.preventionweb.net/understanding-disaster-risk/component-risk/vulnerability,
752 2017.

753 Yunus, A. P., & Narayana, A. C.: Short-term morphological and shoreline changes at Trinkat Island,
754 Andaman and Nicobar, India, after the 2004 tsunami. *Marine Geodesy*, *38*(1), 26-39,
755 https://doi.org/10.1080/01490419.2014.908795, 2015.

756 Yunus, A. P., Dou, J., Avtar, R., & Narayana, A.: Shoreline and coastal morphological changes induced
757 by the 2004 Indian Ocean tsunami in the Katchal Island, Andaman and Nicobar–a study using
758 archived satellite images. In *Tsunamis and earthquakes in coastal environments* (pp. 65-77).
759 Springer, Cham, https://link.springer.com/chapter/10.1007/978-3-319-28528-3_5, 2016.

760 Yuvaraj, E., Saravanan, E., & Dharanirajan, K.: Assessment of land use and land cover changes in south
761 Andaman Island using remote sensing and GIS. *Int J Geomat Geosci*, *5*, 171-181, 2014.

762 Yi, L., Chen, J., Jin, Z., Quan, Y., Han, P., Guan, S., & Jiang, X.: Impacts of human activities on coastal
763 ecological environment during the rapid urbanization process in Shenzhen, China. Ocean &
764 coastal management, 154, 121-132, https://doi.org/10.1016/j.ocecoaman.2018.01.005, 2018.

765